Combustion and Flame 161 (2014) 1131–1134

Contents lists available at ScienceDirect

Combustion and Flame

journal homepage: www.elsevier.com/locate/combustflame

Brief Communications

A mechanistic perspective of atmospheric oxygen sensitivity on composite energetic material reactions

Cory W. Farley [a], Michelle L. Pantoya [a,*], Valery I. Levitas [b]

[a] Department of Mechanical Engineering, Texas Tech University, Lubbock, TX 79424, USA
[b] Iowa State University, Departments of Aerospace Engineering, Mechanical Engineering and Material Science and Engineering, Ames, IA 50011, USA

ARTICLE INFO

Article history:
Received 31 May 2013
Received in revised form 14 September 2013
Accepted 18 October 2013
Available online 12 November 2013

Keywords:
Aluminum combustion
Melt dispersion mechanism
Flame speeds
Energy propagation
Diffusion oxidation

ABSTRACT

Solid energetic composites have been used and studied in standard air environments, yet the contribution of atmospheric oxygen to reactive material combustion has not been investigated. This study experimentally examines the effect of atmospheric oxygen concentration (4% or 93% oxygen) on energy propagation of nanometric aluminum with copper oxide (Al + CuO), iron oxide (Al + Fe_2O_3), calcium iodate (Al + $Ca(IO_3)_2$), and iodine pentoxide (I_2O_5). In all cases energy propagation was examined in terms of flame speed and higher in the high oxygen environments. However, the convectively dominant reactions showed a smaller percent increase in flame speed mainly attributed to the reaction mechanism.

1. Introduction

The influence of oxygen in the atmosphere has been studied for aluminum (Al) combustion either as an aerosolized powder or single Al particles [1–3]. However, there are minimal studies examining the effect of environment on flame speeds of composite fuel and oxidizer powders. Yet, in practice, energetic composites are often used in atmospheric conditions such that the role of oxygen in the environment influencing the combustion should be well understood.

When Al fuel particles are on the nanometric scale and combined with a solid oxidizer, such as a metal oxide, fluoropolymer, or halogen oxide, the flame propagation rate can exceed 100 m/s and sometimes exceed 1000 m/s [4]. For these high heating and flame rates (i.e., speeds >10 m/s), the melt dispersion mechanism (MDM) has been reported to operate [4–7]. Thus, melting of Al is accompanied by a 6% volume increase and produces pressure of several GPa in Al melt and tensile stresses of 10 GPa in the oxide shell, which cause fast fracture and spallation of the shell. Immediately after spallation, pressure inside the liquid Al particle remains the same, while at the bare Al surface it drops almost to zero. This creates an unloading wave with a tensile pressure of 3–8 GPa, which disperses Al particles into a large number of small, bare Al fragments. Oxidation of these fragments is not limited by diffusion through initial oxide shell, which explains extremely high reaction rate. For micron scale Al reactions with a very slow heating rate and flame rates (i.e., <10 m/s) the classical diffusion oxidation mechanism operates [3,8]: reaction rate is limited by diffusion of oxygen and Al toward each other through the growing oxide shell.

This study examines the influence of atmospheric oxygen as a function of reaction mechanism. Experiments are limited to four energetic composites; two representing reaction via the MDM and two via classic diffusion oxidation. The first two composites produce high flame speeds, activate the melt dispersion mechanism, and are composed of aluminum with either copper oxide or iodine pentoxide (Al + CuO and Al + I_2O_5, respectively). It should be noted here that to achieve flame speeds comparable to Al + I_2O_5, the CuO selected for these experiments was on the nanoscale particle size. This enabled us to examine multiple powders with flame speeds greater than 100 m/s that we could classify as "fast burning powders". The second set results in significantly lower flame speeds such that the diffusion oxidation mechanism governs reaction propagation. These composites are aluminum combined with iron oxide or calcium iodate (Al + Fe_2O_3 and Al + $Ca(IO_3)_2$, respectively). These reactions initiate when oxygen is released from the oxide and available to react with the aluminum, however CuO and I_2O_5 dissociate at temperatures near or below the melting temperature of Al while Fe_2O_3 and $Ca(IO_3)_2$ dissociate at higher temperatures [9]. The objective is accomplished through high speed imaging of flame rates in controlled oxygen concentration environments. These experiments are coupled with analytical modeling of

* Corresponding author. Fax: +1 8067423540.
E-mail address: michelle.pantoya@ttu.edu (M.L. Pantoya).

0010-2180/$ - see front matter © 2013 The Combustion Institute. Published by Elsevier Inc. All rights reserved.
http://dx.doi.org/10.1016/j.combustflame.2013.10.018

the alumina passivation shell fracture temperature such that ignition temperatures for the reaction can be correlated to the reaction mechanism.

2. Methods

2.1. Experimental

Passivated aluminum (Al) with a nominal average diameter of 80 nm and an active Al content of approximately 75 wt% was supplied by Novacentrix (formerly Nanotechnologies), Austin, TX. The oxide thickness was calculated to an average 4.0 nm and TEM images of these particles are consistent with this estimation. The Al particles were used for all tests reported here and mixed with either 50 nm average diameter CuO, 40 μm Fe_2O_3, 15 μm $Ca(IO_3)_2$ or I_2O_5 that is ground and sieved through a 355 μm mesh. All powders were supplied by Sigma Aldrich, St. Louis MO or Alfa Aesar, Ward Hill, MA. All reactions were balanced based on oxygen transfer assuming 100% of the oxygen transferred to the Al.

Individual reactant powders were prepared for stoichiometric equivalence ratios. Reactant powders were loaded into a 0.5 by 13 cm notch with a bulk density of 7% of the theoretical maximum density (TMD) of the solid mixture meaning 93% of the volume in the notch is occupied by atmospheric gas. For each test, three to five experiments were performed to establish repeatability, which was found to be the largest source of uncertainty in the data.

The experimental setup includes a sealed combustion chamber with a blow-off valve to prevent pressurization as seen in Fig. 1. Two roughing pumps were connected to the sealed combustion chamber and one third of the atmosphere was vacuumed out and backfilled with either argon (Ar) or oxygen (O_2). This atmospheric cycle was repeated 4 times for the argon and 6 times for the oxygen resulting in a High O_2 content of 93% O_2 by mass and a low O_2 content of 4% by mass. Therefore, when the sample is ignited, the atmosphere is either 4 or 93% O_2 and at atmospheric pressure. Ignition was triggered via a heated nickel chromium hot wire. Flame speeds were recorded via a Phantom 7 high speed camera at frame rates ranging from 900 to 90,000 frames per second aligned perpendicular to the direction of flame propagation. The pixels were converted to millimeters via calibration and combined with the frame rate to calculate flame speed.

2.2. Theoretical

To further understand the influence of reaction mechanism on sensitivity to atmospheric oxygen, the temperature for which oxide shell fractures and melt disperses for Al in a reaction involving MDM can be determined theoretically. The key geometric parameter that governs the MDM is the ratio of Al core, R, to the oxide shell thickness, δ; $M = R/\delta$ For $M < 19$, entire particle melts completely before oxide fracture and entire melt disperses and participate in reaction. The maximum tensile hoop stress in the shell (considered as the negative one) is determined by Eq. (1) [5,10]:

$$\sigma_h = -\frac{6(m^3+2)(\varepsilon_2^i-\varepsilon_1^i)G_2K_1K_2}{H} + \frac{4(m^3+2)G_2K_2\Gamma_1}{RH} + \frac{(2\Gamma_2+p_gRm)m^2(-2G_2K_1+3(2G_2+K_1)K_2)}{RH}, \quad (1)$$

where subscripts 1 and 2 designate Al and alumina, respectively, $m = 1 + 1/M$, Γ_1 and Γ_2 are the surface energies at the core-shell and shell-gas interfaces, G and K are the shear and bulk moduli, $K_1 = fK_1^m + (1-f)K_1^s$ is the bulk modulus of Al melt (m) - solid (s) mixture, f is the concentration of melt in Al particle, and $H = 3m^3K_1K_2 + 4G_2(K_1 + (m^3-1)K_2)$. For convenience, it is assumed that compressive stress is positive and that tensile stress is negative. Inelastic strain consists of thermal and transformational parts:

$$\varepsilon_1^i = -(\alpha_s(T_m - T_0) + (1-f)\alpha_s(T - T_m) + f\alpha_m(T - T_m) + f\varepsilon^m);\ \varepsilon_2^i = -\alpha_2(T - T_0), \quad (2)$$

where α is the linear thermal expansion coefficient, T_0 is the temperature at which the initial oxide shell was formed on the solid Al particle (i.e., temperature at which internal thermal stresses in the solid state are zero), and $3\varepsilon^m$ is the volumetric expansion during the melting of Al. For the MDM, the temperature at which fracture of the oxide shall occurs during continuous heating can be determined from fracture criterion

$$\sigma_h = -\frac{6(m^3+2)(\varepsilon_2^i-\varepsilon_1^i)G_2K_1K_2}{H} + \frac{4(m^3+2)G_2K_2\Gamma_1}{RH} + \frac{(2\Gamma_2+p_gRm)m^2(-2G_2K_1+3(2G_2+K_1)K_2)}{RH} = -\sigma_u \quad (3)$$

by putting $f = 1$, where σ_u is the ultimate strength of alumina. All material parameters are presented in [5]; in particular, $\sigma_{th} = 11.33$ - GPa, $T_0 = 300$ K and $p_g = 0$.

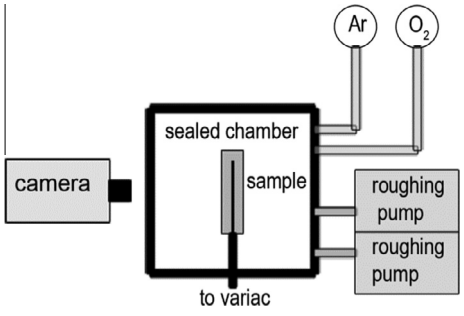

Fig. 1. Experimental schematic for flame speed experiments.

3. Results

Table 1 displays the flame speeds for the mixtures organized by equivalence ratio and atmosphere. In order to compare flame speeds, a percent difference is defined in Eq. (4) where FSH is the flame speed under 93% O_2 conditions and FSL is the flame speed for 4% O_2 conditions.

$$\%\ \text{Increase} = \frac{\text{FSH} - \text{FSL}}{\text{FSL}} * 100\% \quad (4)$$

For 80 nm Al particles used here, $R = 40 - \delta$ and $M = (40 - \delta)/\delta$. Substituting these expressions in Eq. (3) foe the MDM and resolving for T the temperature at which oxide shell fractures versus shell thickness δ is shown in Fig. 2 and can be well approximated by linear relationship in Eq. (5),

$$T = 945 + (\delta - 2)(1449 - 945)/3, \quad (5)$$

which passes through points $T = 945$ K at $\delta = 2$ nm and $T = 1449$ K at $\delta = 5$ nm. In reality, there is a broad range of distribution of particle size and oxide thickness. Even if we assume for

Table 1
Summary of flame speed results from each set of tests with speeds in (m/s).

	Al + I_2O_5	Al + CuO	Al + $Ca(IO_3)_2$	Al + Fe_2O_3
93% O_2	840 ± 40	224 ± 4	2.9 ± 0.04	3.4 ± 0.1
4% O_2	770 ± 20	204 ± 9	2.2 ± 0.05	1.7 ± 0.04
% Increase	9%	10%	30%	100%

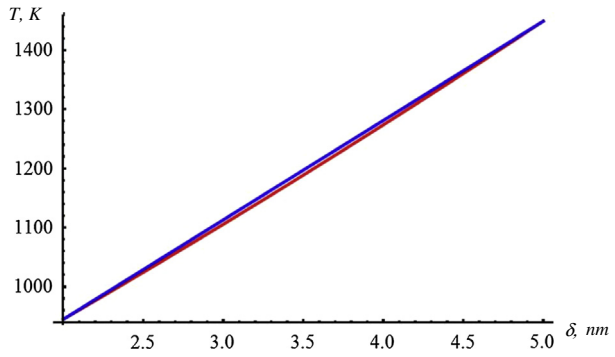

Fig. 2. Temperature which oxide shell for 80 nm Al particle fractures versus shell thickness δ. for the case when MDM operates. Red curve corresponds to nonlinear Eq. (3) and blue curve is a linear approximation Eq. (5). (For interpretation of the references to color in this figure legend, the reader is referred to the web version of this article.)

simplicity constant particle radius of 40 nm, shell thickness may vary and grow during storage of particles. Figure 2 shows that small change in shell thickness significantly affects the temperature at which shell fractures and melt disperses, which can be considered the ignition temperature.

4. Discussion

Jian et al. [9] examined various binary composites and correlated ignition temperatures to oxidizer decomposition temperatures. According to their study, two mixtures used here ignite when their oxidizer begins to decompose. For example, CuO decomposes to Cu_2O at 1000 K and Fe_2O_3 decomposes to Fe_3O_4 at 1400 K [9]. Also, ignition of nanometric Al in a gaseous oxygen environment occurs as low at 1000 K [1]. Thus temperature of CuO decomposition and Al ignition is in the range of the predicted temperature of fracture of the oxide shell and ignition based on the MDM. Before fracture of the shell, diffusion of oxygen toward Al is not significant due to high heating rate provided by MDM and short diffusion time. The decomposition temperature for I_2O_5 is lower than CuO at 390 °C. [11] Therefore, I_2O_5 also is in range of the predicted temperature of fracture of the oxide shell and ignition based on MDM. Therefore, Al + I_2O_5 will be discussed concurrently with Al + CuO as fast burning powders. For the worst case scenario for the fast powders, Al + CuO releases enough O_2 that at the ignition temperature, additional atmospheric oxygen represents only 13% of oxygen available from the oxidizer. Thus, atmospheric oxygen only produces a relatively small contribution to the increase in reactivity and flame velocity. This calculation is based on the following analyses for Al + CuO. Consider 350 mg of powder placed in a 1.4 cm^3 notch resulting in 273 mg CuO for a stoichiometric mixture. Under these conditions, 0.0034 mol of CuO results in the release of 0.0017 mol of oxygen when CuO decomposes to Cu_2O at 1000 K. The volume of atmospheric oxygen in this configuration is estimated to be 2.8 cm^3. Assuming oxygen behaves as an ideal gas in the standard atmosphere, for this volume at a mole fraction of 0.96, 0.00013 mol of O_2 is available for reaction corresponding to 0.00026 mol of O. The percent contribution of atmospheric oxygen can then be estimated from [0.00026/(0.0017 + 0.0026)] × 100% which equals 13%. Similarly, for Al + Fe_2O_3, 40% of available oxygen is atmospheric oxygen when Fe_2O_3 decomposes to Fe_3O_4 at 1400 K assuming no reaction has taken place beforehand.

Therefore, for Al + Fe_2O_3 and the diffusion oxidation mechanism, additional oxygen is the only available oxygen below Fe_2O_3 decomposition temperature of 1400 K. Due to lower heating rate and larger time than for MDM, diffusion occurs through the oxide shell and causes oxidation, leading to an increase in temperature. Note that the rate of reaction is determined by the rate of diffusion and the latter is proportional to the oxygen concentration gradient c_O/δ. Thus, even when oxygen from initial decomposing of Fe_2O_3 is available, the additional atmospheric oxygen increases c_O and consequently the diffusion rate by 40%. Both these contributions (availability of oxygen below 1400 K and essential increase of its concentration above 1400 K) lead to a drastic increase in flame speed (Table 1).

Also, $Ca(IO_3)_2$ decomposes in a two-step process at 825 K and 1050 K. By the time Al reacts with atmospheric oxygen at 1000 K, roughly 50% of the oxygen content is released. With decomposition like this, flame speeds are expected to be comparable to Al + CuO, thus implying an MDM mechanism in the reaction. However, the oxides created in this decomposition are $Ca(IO_3)_2$ and $Ca_5(IO_6)_2$ (e.g., with heats of formation, H_f = 2.57 and 5.92 kJ/g [12]) and much more stable compounds than CuO and Cu_2O (e.g., H_f = 1.95 and 1.17 kJ/g [13]). As a result, even though the decompositions occur at similar temperatures and follow similar steps, the heat absorbed in order to decompose both materials are drastically different. As a result flame speeds are reduced by the decrease in latent heating to the surrounding material. The increase in heat absorption slows the heating rate and allows for more time for diffusion and causes the Al + $Ca(IO_3)_2$ reaction to behave similarly to Al + Fe_2O_3 and not follow MDM as do the faster powders.

Note that all of the results presented here are for flame speeds measured in an open notch configuration. More commonly, flame speeds are reported for a semi-confined burn tube experiment, such that the flame speed for Al + CuO reaches 802 m/s [10]. For the burn tube experiment and for nanoscale Fe_2O_3 oxidizer, flame speed Al + Fe_2O_3 is on the order of 1 km/s [14]. In this case, MDM is expected to operate and the effect of additional oxygen will not be so pronounced. In fact, if the maximum possible flame speed for the given setup is achieved for both mixtures, extra oxygen will likely not affect flame speed and is consistent with results.

5. Conclusions

This study examined the effect of atmospheric oxygen concentration on composite energetic material reactions that are controlled by the melt dispersion mechanism or the diffusion oxidation mechanism. High speed reactions which activate the melt dispersion mechanism show a smaller percent increase in flame speeds when exposed to a high oxygen atmosphere. Slower, diffusion limited reactions showed greater increases in flame speed by as much as 200% increase in a high oxygen atmosphere. A theoretical model for MDM was developed to predict the temperature corresponding to fracture of the alumina shell in reaction and results are consistent with literature reporting experimentally measured ignition temperatures.

Acknowledgments

M. Pantoya and C. Farely gratefully acknowledge support from the Army Research Office contract number W911NF-11-1-0439 and encouragement from our Program Manager Dr. Ralph Anthenien. All authors acknowledge financial support of the Office of Naval Research (Grant N00014-12-1-0525) with Dr. Cliff Bedford as Program Officer.

References

[1] Y. Huang, G.A. Risha, V. Yang, R.A. Yetter, Combust. Flame 156 (1) (2009) 5–13, http://dx.doi.org/10.1016/j.combustflame.2008.07.018.
[2] R.J. Gill, C. Badiola, E.L. Dreizin, Combust. Flame 157 (11) (2010) 2015–2023, http://dx.doi.org/10.1016/j.combustflame.2010.02.023.

[3] R. Friedman, A. Maček, Symp. (Int.) Combust. 9 (1) (1963) 703–712. <http://dx.doi.org/10.1016/S0082-0784(63)80078-8>.
[4] K.W. Watson, M.L. Pantoya, V.I. Levitas, Combust. Flame 155 (4) (2008) 619–634, http://dx.doi.org/10.1016/j.combustflame.2008.06.003.
[5] V.I. Levitas, B.W. Asay, S.F. Son, M. Pantoya, Appl. Phys. Lett. 89 (7) (2006) 071909, http://dx.doi.org/10.1063/1.2335362.
[6] B. Dikici, S.W. Dean, M.L. Pantoya, V.I. Levitas, R.J. Jouet, Energy Fuels 23 (9) (2009) 4231–4235, http://dx.doi.org/10.1021/ef801116x.
[7] V.I. Levitas, B.W. Asay, S.F. Son, M. Pantoya, J. Appl. Phys. 101 (8) (2007) 083524, http://dx.doi.org/10.1063/1.2720182.
[8] K. Park, D. Lee, A. Rai, D. Mukherjee, M.R. Zachariah, J. Phys. Chem. B 109 (15) (2005) 7290–7299, http://dx.doi.org/10.1021/jp048041v.
[9] G. Jian, S. Chowdhury, K. Sullivan, M.R. Zachariah, Combust. Flame 160 (2) (2013) 432–437, http://dx.doi.org/10.1016/j.combustflame.2012.09.009.
[10] V.I. Levitas, M.L. Pantoya, B. Dikici, Appl. Phys. Lett. 92 (1) (2008) 011921, http://dx.doi.org/10.1063/1.2824392.
[11] C. Farley, M. Pantoya, J. Therm. Anal. Calorim. 102 (2) (2010) 609–613, http://dx.doi.org/10.1007/s10973-010-0915-5.
[12] K.H. Stern, in: High Temperature Properties and Thermal Decomposition of Inorganic Salts with Oxyanions, CRC Press, 2000.
[13] T.W. Sottery, J. Chem. Educ. 62 (12) (1985) A325, http://dx.doi.org/10.1021/ed062pA325.
[14] K.B. Plantier, M.L. Pantoya, A.E. Gash, Combust. Flame 140 (4) (2005) 299–309. <http://dx.doi.org/10.1016/j.combustflame.2004.10.009>.